

Co-Design of Reduced-Order Models and Observers from Thermo-Fluid Data

Vijayshankar, Sanjana; Chakrabarty, Ankush; Grover, Piyush; Nabi, Saleh

TR2022-009 February 15, 2022

Abstract

This paper presents a method of co-design of models and observers for buoyancy-driven turbulent flows. Recent work on data-driven techniques for estimating turbulent flows typically involve obtaining a dynamical model using Dynamical Mode Decomposition (DMD) and using the model to design estimators. Unfortunately, such a sequential design could result in state-space models that do not possess control-theoretic properties (such as detectability) that ensure guaranteed performance of the observer. In this paper, we propose semi-definite programs (SDPs) that allow us to simultaneously construct observer gains, along with DMD models which exhibit desired properties. Since DMD models for turbulent flows are typically highdimensional, we provide a tractable algorithm for solving the high-dimensional SDP. We demonstrate the potential of our proposed approach on an industrial application using real-world data, and illustrate that the co-design significantly outperforms sequential design.

IFAC Journal of Systems and Control 2022

Co-Design of Reduced-Order Models and Observers from Thermo-Fluid Data

Sanjana Vijayshankar^{a,**}, Ankush Chakrabarty^b, Piyush Grover^c, Saleh Nabi^{b,*}

^a*Department of Electrical and Computer Engineering, University of Minnesota, Minneapolis, MN 55455, USA.*

^b*Mitsubishi Electric Research Laboratories, Cambridge, MA, USA.*

^c*Department of Mechanical and Materials Engineering, University of Nebraska-Lincoln, NE 68588, USA.*

Abstract

This paper presents a method of co-design of models and observers for buoyancy-driven *turbulent* flows. Recent work on data-driven techniques for estimating turbulent flows typically involve obtaining a dynamical model using Dynamical Mode Decomposition (DMD) and using the model to design estimators. Unfortunately, such a sequential design could result in state-space models that do not possess control-theoretic properties (such as detectability) that ensure guaranteed performance of the observer. In this paper, we propose semi-definite programs (SDPs) that allow us to simultaneously construct observer gains, along with DMD models which exhibit desired properties. Since DMD models for turbulent flows are typically high-dimensional, we provide a tractable algorithm for solving the high-dimensional SDP. We demonstrate the potential of our proposed approach on an industrial application using real-world data, and illustrate that the co-design significantly outperforms sequential design.

Keywords: Co-design, state estimation, data-driven methods, linear matrix inequalities, partial differential equations, turbulent flows, model order reduction

1. Introduction

Buildings contribute around 40% of the energy consumption in the United States. Building simulation involves simulating thermo-fluid systems that couple dynamical information from heating, ventilation and air-conditioning (HVAC) equipment along with airflow within the built environment. Building dynamics are typically complex, multi-rate, multi-scale, multi-physics, and subject to a wide variety of exogenous disturbances and systemic uncertainties [1, 2]. Designing computationally tractable tools for analysis and synthesis of controllers and estimators for energy-efficient buildings is a challenging problem due to inherent complexity of building dynamics [3]. A critical component of building models includes dynamics contributed by thermo-fluid systems such as those produced by airflow systems.

A realistic model for describing airflow dynamics employs the Boussinesq equations, which are nonlinear partial differential equations (PDEs) [4, 5], that combine the Navier-Stokes (NS) equation and heat transfer equations. Since closed-form solutions to such PDEs are generally impossible to find, the Boussinesq equations are solved numerically. Numerical simulations are performed by discretizing in space and marching in time. This meshing approach usually generates large-scale discrete-time systems, where the state-variables describe local dynamics on the mesh nodes; therefore, it is not uncommon for the state-space to be 10^4 to 10^6 dimensional, even for low- to medium-resolution grids. Since such massive state-spaces are intractable for controller and estimator design, this motivates the use of data-driven reduced-order models (ROMs)

*Corresponding author. Phone: +1 (617) 621-7589.

**This work was completed during an internship at MERL.

Email addresses: vijay092@umn.edu (Sanjana Vijayshankar), chakrabarty@merl.com (Ankush Chakrabarty), piyush.grover@unl.edu (Piyush Grover), nabi@merl.com (Saleh Nabi)

for efficient simulation of the system dynamics, wherein the data is generated from physics-informed simulations [6]. One reduced-order modeling technique that has gained popularity in the fluid dynamics and control community is the Dynamic Mode Decomposition (DMD) [7, 8, 9]. DMD employs singular-value decomposition (SVD) to efficiently fit a linear evolution model to high-dimensional snapshot data. DMD provides an approximation of the Koopman operator – a linear but infinite dimensional operator that governs the time evolution of scalar functions defined on the state space. DMD can be shown to be a faithful representation of the Koopman operator under some assumptions [10].

In addition to an appropriate reduced-order model, one also needs observers so that measurements obtained from spatially local subregions of the space of interest can be used to glean spatially global state information, which can be fed to control algorithms. Therefore, observer design is critical for the design pipeline in thermo-fluid systems. A few ROM-based state observers have been proposed for the Navier-Stokes equation, see for example [11, 12, 13]. For the Boussinesq equation, far fewer estimation results are available due to the presence of a coupling nonlinearity between the NS equation and the thermal equation. This nonlinearity makes the estimation problem significantly more challenging and standard linear observers difficult to construct or limited in use even after construction. In [14], the authors proposed a learning-based robust observer design for the two-dimensional Boussinesq equation under model parametric uncertainties. They proved that the closed loop system for the observer error state satisfies an estimate of \mathcal{L}_2 norm in a sense of locally input-to-state stability (L-ISS) with respect to parameter uncertainties. Then they proposed to learn the uncertain parameters estimate using a data-driven extremum seeking (ES) algorithm, and more recently, using Bayesian optimization [15]. In [16], the authors introduced a method for designing robust, proper orthogonal decomposition (POD)-based, low-order observers for a class of infinite-dimensional nonlinear systems, with application to the 2D Boussinesq equation. Robustness to bounded model uncertainties was incorporated using the Lyapunov reconstruction approach from robust control theory. The gains of the observer were optimized online using a data-driven learning approach. Other approximators, such as neural networks for learning-based observer design has been investigated in [17]. In our previous work [18], we developed a sequential algorithm for designing \mathcal{H}_∞ and Kalman filters based on a state-space representation obtained using DMD.

While sequential algorithms have demonstrated success, they possess a fundamental problem: in sequential design, *one cannot impose explicit control-theoretic properties on the models such as observability or controllability*. However, such conditions are crucial for subsequent design and synthesis: obtaining a DMD-based ROM that is not controllable or observable will break the controller design pipeline, as no linear state-feedback will exist to drive the system to a desired state. To overcome this fundamental limitation of sequential designs, recent research has proposed co-design formulations that exhibit high performance [19, 20]. The most common application of co-design is to shift poles and zeros of the system into desired regions of the complex domain to provide certificates on closed-loop control performance [21]. Co-design has also been applied to mechanical engineering and aerospace engineering systems, including vehicles [22, 23, 24], combined heat and power systems [25], aircraft [26], and chemical engineering systems such as mixing tanks [27]. Very recently, co-design has been explored in thermo-fluid systems to tradeoff nominal (steady-state) efficiency with transient efficiency while also ensuring robustness to highly transient disturbances via nonlinear parameterized models [28, 29]. However, to the best of our knowledge, the co-design of DMD-based models and observers *from simulation data* has not been explored prior to this work; prior art has always tackled the co-design problem by assuming complete knowledge of the full-order model.

In this paper, we use CFD simulation data directly to construct reduced-order models and state observers simultaneously in a co-design framework. We propose new sufficient conditions for designing the model and observer pair, and ensure detectability of the identified system. We also provide computationally tractable algorithms based on Burer-Monteiro approaches [30] that can solve the main semidefinite program proposed in this work. Our contributions in this paper are as follows: (i) To the best of our knowledge, this paper contains the first data-driven formulation of state and observer co-design for systems whose dynamics are described by partial differential equations. Note that the data used for our method could be obtained by experiments or computational fluid dynamics simulations. (ii) Since turbulent flow dynamics typically reside in large state-spaces, our proposed SDP-based solution has a large number of variables. Furthermore, it is well-known that simultaneous co-design of models and controllers/estimators results in

non-convex, large-scale optimization problems, and approximations are typically required to solve them in polynomial time [28]. To this end, we propose the use of Burer-Monteiro methods to solve the large SDPs that arise in our simultaneous co-design formulation. (iii) We numerically validate the proposed co-design framework for turbulent flows using data obtained from a real-world industrial air conditioning application, and demonstrate instabilities arising from sequential design, even in simple scenarios.

The rest of the paper is organized as follows. In Section 2, we present two PDE models for airflow dynamics: a simpler Advection-Diffusion model which describes temperature dynamics, and the more complex Boussinesq equations used to describe the temperature and velocity of turbulent flows. We also formally present the problem and proposed solution. In Section 3, we present the sequential method of ROM-based estimator design. The proposed co-design framework is explained in Section 4, and methods for solving the large-scale SDPs arising in this framework is also presented there. We demonstrate the potential of our method in optimizing modeling and estimation of thermo-fluid systems in Section 5 via real-world examples of turbulent flows in industrial buildings and warehouses. We provide concluding remarks in Section 6.

2. Background and Motivation

2.1. PDE Models for Airflow Dynamics

We use two well-known PDE-based models of thermo-fluid flows in building systems to test the algorithms developed in this work. Our proposed methodology is generalizable to other PDEs since it is data-driven and does not depend on the details of the PDE. The first model is given by the linear advection-diffusion equation – a scalar-valued PDE that describes the time evolution of the temperature distribution in a domain. This simplified description ignores the effect of non-uniform temperature distribution on the air velocity. A steady velocity field consisting of a double vortex is used in this model. The second model is given by the Boussinesq equations – a nonlinear vector-valued PDE which is a realistic representation of airflow in a room, since it models the two-way coupled evolution of temperature and velocity distributions. The two models are now described in further detail.

2.1.1. Advection-Diffusion Equation Based Model

We consider airflow in a closed room modeled as a 2D domain $\Omega \subset \mathbb{R}^2$, with boundary denoted by $\partial\Omega$. The temperature field $T((x, y), t) : \Omega \times \mathbb{R}_+ \rightarrow \mathbb{R}$ evolves under the combined action of advection by a velocity field $\mathbf{v}((x, y), t) : \Omega \times \mathbb{R}_+ \rightarrow \mathbb{R}^2$, and diffusion. The velocity field is an incompressible vector field that comprises of two counter-rotating vortices, given explicitly by

$$\mathbf{v} = \sin(\pi x) \cos(\pi y) \mathbf{i} - \cos(\pi x) \sin(\pi y) \mathbf{j}, \quad (1)$$

where \mathbf{i} , \mathbf{j} are unit vectors in the horizontal and vertical directions, respectively. The advection-diffusion PDE expressed in the Einstein notation is

$$0 = \frac{\partial T}{\partial t} + T \frac{\partial v_j}{\partial x_j} - \frac{\partial}{\partial x_j} \left(\frac{1}{Pe} \frac{\partial T}{\partial x_j} \right), \quad (2)$$

where the Peclet number $Pe = v_c L_c / \kappa$, and L_c and v_c are the characteristic length and velocity scales of the problem, respectively. The boundary conditions are given by

$$T(\partial\Omega_1, t) = T_b, \quad (3a)$$

$$n_i \frac{\partial T(\partial\Omega_2, t)}{\partial x_i} = 0, \quad (3b)$$

where \mathbf{n} is the unit normal vector. Here, the boundary is split into two components, i.e., $\partial\Omega = \partial\Omega_1 \cup \partial\Omega_2$, where $\partial\Omega_1$ is the boundary component with Dirichlet boundary conditions, and $\partial\Omega_2$ is the boundary component with no-flux Neumann boundary conditions. In our case study, $\partial\Omega_1$ is comprised of the top and bottom surfaces, and $\partial\Omega_2$ is comprised of the the lateral walls.

2.1.2. Boussinesq Equations Based Model

We consider airflow in a 2D slice of a real environment with an inlet and an outlet. Fig. 1 illustrates a snapshot of such a flow using temperature colored streamlines. Cold air enters the room through a distributed inlet (diffuser) at the top vent Γ_i , subject to Dirichlet boundary conditions of prescribed inlet velocity and temperature. The air leaves the room through an exhaust located at the top left corner of the domain Γ_o , subject to zero-Neumann boundary conditions. The model is described by the Boussinesq

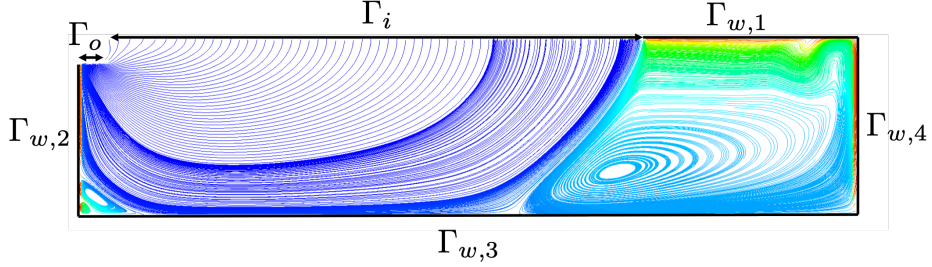


Figure 1: Exemplar solution of the 2-D Boussinesq equation in a representative built environment.

system of equations, consisting of incompressible Navier-Stokes equations governing the 2D velocity field, coupled with the advection-diffusion equation governing the scalar temperature distribution. In Einstein notation, the equations are

$$0 = \frac{\partial u_j}{\partial x_j}, \quad (4a)$$

$$0 = \frac{\partial u_i}{\partial \tau} + \frac{\partial u_i u_j}{\partial x_j} + \frac{\partial p_i}{\partial x_i} - Ri \delta_{i2} T - \frac{\partial}{\partial x_j} \left(\frac{1}{Re} \frac{\partial u_i}{\partial x_j} \right), \quad (4b)$$

$$0 = \frac{\partial T}{\partial \tau} + \frac{\partial u_j T}{\partial x_j} - \frac{\partial}{\partial x_j} \left(\frac{1}{Pe} \frac{\partial T}{\partial x_j} \right), \quad (4c)$$

where \mathbf{u}, p, T are scaled ensemble-averaged velocity, pressure, and temperature respectively, and δ_{ij} is the Kronecker delta. Non-dimensional numbers in (4) are given by

$$Re = \frac{u_{c,in} L_{c,in}}{\nu_{eff}}, \quad Pe = \frac{u_{c,in} L_{c,in}}{\kappa_{eff}}, \quad Ri = \frac{u_{c,in} \theta_{c,in} L_{c,in}}{V_{in}^2},$$

where subscript ‘in’ denotes the values at the inlet. The effective viscosity and diffusivity are ν_{eff} and κ_{eff} , respectively, and are computed by unsteady Reynolds-averaged Navier Stokes (RANS) approach, in which there is a scale separation between the unsteadiness of the mean flow and the turbulence. The closure of (4) are k - ϵ equations to model the Reynolds stress and turbulent heat flux. Consequently, the closure is used

to determine ν_{eff} and κ_{eff} [31]. Boundary conditions are provided as follows:

$$\text{Inlet :} \quad \Gamma_i = \begin{cases} \mathbf{u} \cdot \mathbf{n} & = u_{\text{in}}, \\ \mathbf{u} - \mathbf{u} \cdot \mathbf{n} & = 0, \\ T & = T_{\text{in}}, \\ n_j \frac{\partial p}{\partial x_j} & = 0, \end{cases} \quad (5a)$$

$$\text{Outlet :} \quad \Gamma_o = \begin{cases} n_j \frac{\partial u_i}{\partial x_j} & = 0, \\ n_j \frac{\partial T}{\partial x_j} & = 0, \\ p & = 0, \end{cases} \quad (5b)$$

$$\text{Wall :} \quad \bigcup_{k=1}^4 \Gamma_{w,k} = \begin{cases} \mathbf{u} & = 0, \\ T & = T_{\text{wall}}, \\ n_j \frac{\partial p}{\partial x_j} & = 0, \end{cases} \quad (5c)$$

where \mathbf{n} is the unit vector normal to the surface. The exterior serves as the heat source for the domain by prescribing temperature at boundaries $\Gamma_{w,1}-\Gamma_{w,4}$. In practice, the wall temperature T_{wall} is not known and is modeled as a disturbance input. Note that this disturbance input rarely conforms to standard stochastic distributions (*e.g.* Gaussian) because it depends on ambient/exterior temperatures, wall material, amongst other factors, and therefore requires careful selection of robust estimators.

2.2. Problem Statement and Proposed Solution

Due to the infinite-dimensionality of systems described by PDEs, and the nonlinearity of, for example, the Boussinesq equations, it is difficult to directly use the PDE equations to generate state estimators or observers. However, due to space and expense limitations, only fixed-points in space have sensors installed, and therefore, only a few locations of temperature and velocity are measured in real-time. However, real-world applications require state estimators or observers to study the overall dynamics of these flows so that the flows can be subsequently controlled via state-feedback.

Offline, we can use archived data obtained from sensors and actuators in a building (such as temperature and velocity sensors and HVAC equipment as actuators) or run high-fidelity computational fluid dynamics (CFD) simulations in order to obtain a dataset \mathcal{D} . Online, however, such spatial data is impossible to collect in real-time, and therefore, a predictive model and state observer is required to ascertain the state of the system.

The dataset \mathcal{D} typically comprises of time series data which can be used to construct a reduced-order model $\mathcal{M} : \mathcal{X} \times \mathcal{U} \rightarrow \mathcal{X} \times \mathcal{Y}$, where $\mathcal{X} \subseteq \mathbb{R}^{n_x}$ is the ambient state-space induced by the ROM, $\mathcal{U} \subseteq \mathbb{R}^{n_u}$ is the admissible set of control inputs, and $\mathcal{Y} \subseteq \mathbb{R}^{n_y}$ is the set of measurements that can be obtained real-time in the building. Since $n_y < n_x$, we will also construct an estimator/observer $\mathcal{E} : \mathcal{Y} \times \mathcal{U} \rightarrow \mathcal{X}$ that is capable of reconstructing the states of the dynamical system with exponentially stable error decay. In the sequential design procedure, one designs \mathcal{M} and then leverages this ROM to design \mathcal{E} ; see for example, [18].

While sequential design methods are both common and perform well under most circumstances, they do not always ensure that the final \mathcal{M} and \mathcal{E} together satisfy desired properties [32]. For instance, one may wish to design a \mathcal{E} such that the pair $(\mathcal{M}, \mathcal{E})$ satisfies detectability conditions or such that the combination maximizes disturbance rejection. *We posit that incorporating such desirable properties into the design requires co-design.* Co-design involves simultaneously searching for both \mathcal{M} and \mathcal{E} such that the combination of systems exhibits prescribed performance guarantees.

Concretely, we assume the availability of an ordered time-series of data snapshots $\{\mathbf{x}_k, \mathbf{u}_k\}_{k=0}^m$ obtained from high-fidelity CFD simulations of a thermo-fluid system, where k is a time index. We assume there exists a mesh on which the CFD simulations have been constructed, and that the state variables of the system are associated with nodes on the mesh. In particular, the k -th snapshot is comprised of column vectors of measured states $\mathbf{x}_k \in \mathbb{R}^{n_x}$ and inputs $\mathbf{u}_k \in \mathbb{R}^{n_u}$, and $(m+1) \in \mathbb{N}$ denotes the total number of snapshots. We also assume that the data is available in its entirety during design time, and has been

collected in such a way that the dynamics are excited and therefore, non-trivial. Using this data, we aim to construct a discrete-time model of the form

$$\mathbf{x}_{k+1} = \mathbf{A}\mathbf{x}_k + \mathbf{B}\mathbf{u}_k, \quad (6a)$$

$$\mathbf{y}_k = \mathbf{C}\mathbf{x}_k \quad (6b)$$

such that the approximation error

$$\|\mathbf{x}_{k+1} - \mathbf{A}\mathbf{x}_k - \mathbf{B}\mathbf{u}_k\|_F \quad (7)$$

is minimized over all snapshots.

In (6), the system matrix \mathbf{A} is of size $n_x \times n_x$, the input matrix \mathbf{B} is of size $n_x \times n_u$, and the output measurement matrix \mathbf{C} is of size $n_y \times n_x$. We make the following assumptions on the system to ensure that the system identification problem is well-posed.

Assumption 1. The state-space dimensions n_x , n_u , and n_y are known. The matrix \mathbf{C} is known. There exists some \mathbf{A} such that the pair (\mathbf{A}, \mathbf{C}) is observable. The input sequence \mathbf{u}_k is persistently exciting.

Assumption 1 is relatively mild. Since the mesh on which the simulation data from CFD simulations are known, and states are defined on nodes, the total number of states are easy to compute. In most practical applications, the number of inputs and measurements are known. The knowledge of the output matrix is stronger, but since the underlying mesh is assigned on the domain Ω of interest, and each state is assigned to a node, the knowledge of \mathbf{C} is equivalent to knowing which node(s) in Ω have sensors installed in them, i.e., this knowledge is provided at design time by a sensor placement algorithm. Finally, persistently exciting inputs are well-known to be necessary for identifying dynamical systems, see for example, [33].

In the sequel, we propose a co-design strategy for synthesis of system matrices and observer gains for fluid flow problems using a non-convex optimization method, ensuring that the error dynamics of the observer are asymptotically stable. We cast this original problem as a semidefinite program (SDP). To provide tractability when the ROM also needs to be large to yield desired approximation properties to the given data, we convert this problem to a unconstrained non-convex problem which allows us to use scalable optimization algorithms.

3. Sequential Design

In sequential (classical) design, we first construct reduced-order models (ROMs) based on experimental or simulated data. Subsequent to the system identification phase, we construct an observer based on the ROM matrices. In particular, we employ DMDc for constructing the ROM and standard linear matrix inequalities for generating the observer gains. This section provides a brief discussion of both DMDc and the observer design.

Unfortunately, the full-order model (6) may not always be amenable to analysis or design, since PDEs of turbulent flows are represented using high-resolution discretization of space, that in turn result in excessively large n_x . Therefore, it becomes necessary to design ROMs of lower state-space dimension; i.e., $r_x \leq n_x$. In particular, dynamic mode decomposition with control (DMDc) yields a ROM of the form

$$\hat{\mathbf{x}}_{k+1} = \hat{\mathbf{A}}_s \hat{\mathbf{x}}_k + \hat{\mathbf{B}}_s u_k, \quad (8)$$

where $\hat{\mathbf{x}} \in \mathbb{R}^{r_x}$, $u \in \mathbb{R}^{n_u}$, are reduced-order states and inputs, respectively. The reduced-order system matrices $\hat{\mathbf{A}}_s$ and $\hat{\mathbf{B}}_s$ have dimensions $r_x \times r_x$ and $r_x \times n_u$, respectively, and are tractable for analysis and design.

We now briefly describe how to generate this ROM with DMDc; for more details, we refer the reader to [34]. Let

$$\mathbf{X}_+ = [\mathbf{x}_1 \quad \mathbf{x}_2 \quad \cdots \quad \mathbf{x}_m], \quad (9a)$$

$$\mathbf{X} = [\mathbf{x}_0 \quad \mathbf{x}_1 \quad \cdots \quad \mathbf{x}_{m-1}], \text{ and} \quad (9b)$$

$$\mathbf{U} = [\mathbf{u}_0 \quad \mathbf{u}_1 \quad \cdots \quad \mathbf{u}_{m-1}] \quad (9c)$$

denote data matrices constructed using the available snapshots. By construction, we obtain

$$\mathbf{X}_+ = \mathbf{A}_s \mathbf{X} + \mathbf{B}_s \mathbf{U}, \quad (10)$$

which can be rewritten as

$$\mathbf{X}_+ = [\mathbf{A}_s \quad \mathbf{B}_s] \begin{bmatrix} \mathbf{X} \\ \mathbf{U} \end{bmatrix} =: \bar{\mathbf{A}}_s \bar{\mathbf{X}}. \quad (11)$$

Note that the augmented matrix $\bar{\mathbf{X}}$ is of size $(n_x + n_u) \times m$.

We deduce from (10) that minimizing the approximation error (7) is tantamount to minimizing $\|\mathbf{X}_+ - \bar{\mathbf{A}}_s \bar{\mathbf{X}}\|_F$.

We take a truncated SVD of $\bar{\mathbf{X}}$ up to a truncation value of $r' > r_x$, that is $\bar{\mathbf{X}} \approx \bar{\mathbf{U}} \bar{\Sigma} \bar{\mathbf{V}}^\top$, where $\bar{\Sigma}$ has r' non-zero diagonal entries. This yields $\bar{\mathbf{A}}_s \approx \mathbf{X}_+ \bar{\mathbf{V}} \bar{\Sigma}^{-1} \bar{\mathbf{U}}^\top$. The matrix $\bar{\mathbf{A}}_s$ can be partitioned into the state and input matrices \mathbf{A}_s and \mathbf{B}_s described in (6) as follows:

$$[\mathbf{A}_s \quad | \quad \mathbf{B}_s] = [\mathbf{X}_+ \bar{\mathbf{V}} \bar{\Sigma}^{-1} \bar{\mathbf{U}}_1^\top \quad | \quad \mathbf{X}_+ \bar{\mathbf{V}} \bar{\Sigma}^{-1} \bar{\mathbf{U}}_2^\top], \quad (12)$$

where $\bar{\mathbf{U}}_1 \in \mathbb{R}^{n_x \times r'}$ and $\bar{\mathbf{U}}_2 \in \mathbb{R}^{n_u \times r'}$.

As explained earlier, the ambient state space n_x may be prohibitively large for estimator and controller design. Therefore, we need an additional projection step to bring this state-dimension down to r_x . The target state dimension r_x is a design parameter. One heuristic that is commonly used to inform the selection of r_x is by generating the spectrum of \mathbf{X}_+ and selecting r_x based on the cumulative concentration of DMD modes, for example, by only considering singular values that contribute 99% of the variance. Unlike conventional DMD, we cannot use $\bar{\mathbf{U}}$ to find the projection subspace basis because $\bar{\mathbf{U}}$ contains both state and input data. Instead, we find the basis from the pure state data matrix \mathbf{X}_+ . This involves computing another truncated SVD, that is,

$$\mathbf{X}_+ = \hat{\mathbf{U}} \hat{\Sigma} \hat{\mathbf{V}}^\top,$$

where $\hat{\Sigma}$ has r_x non-zero diagonal elements due to truncation. The projected state is then given by

$$\hat{\mathbf{x}} := \hat{\mathbf{U}}^\top \mathbf{x}. \quad (13a)$$

Consequently, the reduced-order system matrices are computed using

$$\hat{\mathbf{A}}_s = \hat{\mathbf{U}}^\top \bar{\mathbf{A}}_s \hat{\mathbf{U}} = \hat{\mathbf{U}}^\top \mathbf{X}_+ \bar{\mathbf{V}} \bar{\Sigma}^{-1} \bar{\mathbf{U}}_1^\top \hat{\mathbf{U}}, \quad (13b)$$

$$\hat{\mathbf{B}}_s = \hat{\mathbf{U}}^\top \bar{\mathbf{B}}_s = \hat{\mathbf{U}}^\top \mathbf{X}_+ \bar{\mathbf{V}} \bar{\Sigma}^{-1} \bar{\mathbf{U}}_2^\top. \quad (13c)$$

This, along with $\hat{\mathbf{u}} := \mathbf{u}$ yields the desired reduced-order model (8).

The ROM (8) is also equipped with the measurement output equation

$$\mathbf{y}_k = \hat{\mathbf{C}}_s \hat{\mathbf{x}}_k, \quad (14)$$

where $\hat{\mathbf{C}}_s := \mathbf{C} \hat{\mathbf{U}}$ is a $n_y \times r_x$ measurement matrix, and \mathbf{y} is the measured output. Note that this computation is possible because (by Assumption 1), we know the output matrix \mathbf{C} .

With the ROM matrices available, we can now design a discrete-time Luenberger observer of the form

$$\mathbf{z}_{k+1}^s = \hat{\mathbf{A}}_s \mathbf{z}_k^s + \hat{\mathbf{B}}_s \hat{\mathbf{u}}_k + \hat{\mathbf{L}}_s (\hat{\mathbf{C}}_s \mathbf{z}_k^s - \mathbf{y}_k), \quad (15)$$

with the observer gain $\hat{\mathbf{L}}_s$. It is well known [35] that observer gain can be designed by computing a positive definite matrix $\hat{\mathbf{P}}$ such that

$$\mathbf{P} - (\hat{\mathbf{A}}_s + \hat{\mathbf{L}}_s \hat{\mathbf{C}}_s) \mathbf{P} (\hat{\mathbf{A}}_s + \hat{\mathbf{L}}_s \hat{\mathbf{C}}_s)^\top \succ 0.$$

Taking Schur complements of this matrix inequality yields

$$\begin{bmatrix} \mathbf{P} & (\hat{\mathbf{A}}_s + \hat{\mathbf{L}}_s \hat{\mathbf{C}}_s) \mathbf{P} \\ \star & \mathbf{P} \end{bmatrix} \succ 0, \quad (16)$$

where the ‘ \star ’ notation implies that the matrix is symmetric. Performing a congruent transformation with \mathbf{P}^{-1} , we get

$$\begin{bmatrix} \mathbf{P}^{-1} & \mathbf{P}^{-1}(\hat{\mathbf{A}}_s + \hat{\mathbf{L}}_s \hat{\mathbf{C}}_s) \\ \star & \mathbf{P}^{-1} \end{bmatrix} \succ 0.$$

Substituting $\mathbf{P}_s = \mathbf{P}^{-1}$ and $\hat{\mathbf{Q}}_s = \mathbf{P}^{-1} \hat{\mathbf{L}}_s$ yields the linear matrix inequality (LMI)

$$\begin{bmatrix} \mathbf{P}_s & \mathbf{P}_s \hat{\mathbf{A}}_s + \hat{\mathbf{Q}}_s \hat{\mathbf{C}}_s \\ \star & \mathbf{P}_s \end{bmatrix} \succeq 0, \quad (17)$$

in $\mathbf{P}_s \succ 0$ and $\hat{\mathbf{Q}}_s$, which can be solved by standard semidefinite programming solvers, as long as r_x is small (empirically, < 50 ROM states). Such a design ensures that the state estimation error with the observer gain $\hat{\mathbf{L}}_s = \mathbf{P}_s \hat{\mathbf{Q}}_s$ is asymptotically stable, i.e., the estimate $\mathbf{z}_k^s \rightarrow \hat{\mathbf{x}}_k$ as $k \rightarrow \infty$.

Pseudocode for sequential design is provided in Algorithm 1.

Algorithm 1 Sequential Design

Require: Data, \mathbf{X}_+ , $\bar{\mathbf{X}}$
Require: Output matrix, \mathbf{C}
Require: Target state dimension, r_x
Require: Truncation value, $r' > r_x$
Require: Truncated SVD subroutine, $[\mathbf{U}, \Sigma, \mathbf{V}] = \text{svd}(\cdot, \cdot)$
 $[\bar{\mathbf{U}}, \sim, \sim] = \text{svd}(\bar{\mathbf{X}}, r')$
Partition $\bar{\mathbf{U}} = [\bar{\mathbf{U}}_1 \quad \bar{\mathbf{U}}_2]$
Compute \mathbf{A}_s and \mathbf{B}_s as in (12)
 $[\hat{\mathbf{U}}, \sim, \sim] = \text{svd}(\mathbf{X}_+, r_x)$
Compute $\hat{\mathbf{A}}_s$ using (13b)
Compute $\hat{\mathbf{B}}_s$ using (13c)
Compute $\hat{\mathbf{C}}_s$ using (14)
Solve the LMI (17) for $\mathbf{P}_s \succ 0$, $\hat{\mathbf{Q}}_s$
Compute $\hat{\mathbf{L}}_s = \mathbf{P}_s \hat{\mathbf{Q}}_s$
return $\hat{\mathbf{A}}_s, \hat{\mathbf{B}}_s, \hat{\mathbf{C}}_s, \hat{\mathbf{L}}_s$

4. Model and Observer Co-Design

In this section, we propose a co-design method to simultaneously identify the system matrices and observer gains directly from data; the co-design is done offline. The sequential design may result in an $\hat{\mathbf{A}}_s$ matrix for which the pair $(\hat{\mathbf{A}}_s, \hat{\mathbf{C}}_s)$ is not observable, and therefore, no feasible solution to (17) will exist. This is a fundamental problem that can break down the pipeline for subsequent controller design. In our proposed co-design framework, we ensure that the identified system is observable, and that an observer is guaranteed to exist.

4.1. System/Observer Co-Design

In the co-design setting, we assume that, like the sequential design, we have the snapshot data, and therefore, we can perform SVD in order to compute the lower-dimensional data snapshot matrices. That is, we have access to \mathbf{X}_+ , \mathbf{X} , and \mathbf{U} , as per (9), and with $\hat{\mathbf{U}}$ we can compute $\hat{\mathbf{C}}_s$, as described in (14). We have an additional assumption to enable the co-design; in practice, this assumption is mild.

Assumption 2. The matrix $[\mathbf{X}^\top \quad \mathbf{U}^\top]^\top$ has full row rank.

In order to make this co-design tractable, we modify the original system identification cost function (7) to the following weighted cost:

$$\mathbf{J}_c = \left\| \mathbf{W}_L \left(\mathbf{X}_+ - [\hat{\mathbf{A}}_c \quad \hat{\mathbf{B}}_c] \begin{bmatrix} \mathbf{X} \\ \mathbf{U} \end{bmatrix} \right) \mathbf{W}_R \right\|_F^2, \quad (18)$$

where the system matrices $\mathbf{A}_c \in \mathbb{R}^{n_x \times n_x}$ and $\mathbf{B}_c \in \mathbb{R}^{n_x \times n_u}$ are the matrices to be identified in the co-design, and \mathbf{W}_L and \mathbf{W}_R are the weighting matrices. The role of the weighting matrices is to enable a convex relaxation of the co-design problem, as we shall see in this subsection. We reiterate that solving the problem (18) could result in an \mathbf{A}_c matrix such that $(\mathbf{A}_c, \hat{\mathbf{C}}_s)$ is not observable. In order to co-design \mathbf{A}_c and an observer gain \mathbf{L}_c we can follow the same arguments made in the previous section, and rewrite (16) as

$$\begin{bmatrix} \mathbf{P} & (\hat{\mathbf{A}}_c + \hat{\mathbf{L}}_c \hat{\mathbf{C}}_s) \mathbf{P} \\ \mathbf{P}(\hat{\mathbf{A}}_c + \hat{\mathbf{L}}_c \hat{\mathbf{C}}_s)^\top & \mathbf{P} \end{bmatrix} \succ \mathbf{0}. \quad (19)$$

by replacing $\hat{\mathbf{A}}_s, \hat{\mathbf{L}}_s$ with $\hat{\mathbf{A}}_c, \hat{\mathbf{L}}_c$.

Let

$$\mathbf{W}_R = \begin{bmatrix} \mathbf{X} \\ \mathbf{U} \end{bmatrix}^\ddagger \quad \text{and} \quad \mathbf{W}_L = \begin{bmatrix} \mathbf{P}^{-1} & \mathbf{0} \\ \mathbf{0} & \mathbf{I} \end{bmatrix}, \quad (20)$$

where $(\cdot)^\ddagger$ denotes the Moore-Penrose pseudoinverse operator. Note that \mathbf{W}_R exists because of Assumption 2, and \mathbf{W}_L exists because $\mathbf{P} \succ \mathbf{0}$. Substituting \mathbf{W}_R and \mathbf{W}_L from (20) in (18), yields the equivalent modeling cost function

$$\mathbf{J}_c = \left\| \begin{bmatrix} \mathbf{P}^{-1} & \mathbf{0} \\ \mathbf{0} & \mathbf{I} \end{bmatrix} \left(\mathbf{X}_+ \begin{bmatrix} \mathbf{X} \\ \mathbf{U} \end{bmatrix}^\ddagger - [\hat{\mathbf{A}}_c \quad \hat{\mathbf{B}}_c] \right) \right\|_F^2. \quad (21)$$

Let

$$[\mathbf{X}_1 \quad | \quad \mathbf{X}_2] := \mathbf{X}_+ \begin{bmatrix} \mathbf{X} \\ \mathbf{U} \end{bmatrix}^\ddagger, \quad (22)$$

where $\mathbf{X}_1 \in \mathbb{R}^{n_x \times n_x}$ and $\mathbf{X}_2 \in \mathbb{R}^{n_x \times n_u}$. Minimizing the cost (21) is equivalent to minimizing its components

$$\begin{aligned} \mathbf{J}_{c,1}(\hat{\mathbf{A}}_c) &:= \|\mathbf{P}^{-1}(\mathbf{X}_1 - \hat{\mathbf{A}}_c)\|_F^2, \\ \mathbf{J}_{c,2}(\hat{\mathbf{B}}_c) &:= \|\mathbf{X}_2 - \hat{\mathbf{B}}_c\|_F^2. \end{aligned} \quad (23)$$

Clearly, the optimal $\hat{\mathbf{B}}_c = \mathbf{X}_2$.

Our proposed sufficient condition required for the co-design, i.e., to obtain both a state matrix $\hat{\mathbf{A}}_c$ that minimizes (23) and is guaranteed to form an observable pair with $\hat{\mathbf{C}}_s$ can be obtained by solving the optimization problem

$$\begin{aligned} \min_{\mathbf{P}, \hat{\mathbf{A}}_c, \mathbf{L}_c} \quad & \|\mathbf{P}^{-1}(\mathbf{X}_1 - \hat{\mathbf{A}}_c)\|_F^2 \\ \text{subject to:} \quad & \begin{bmatrix} \mathbf{P}^{-1} & \mathbf{P}^{-1}\hat{\mathbf{A}}_c + \mathbf{P}^{-1}\hat{\mathbf{L}}_c\hat{\mathbf{C}}_s \\ \star & \mathbf{P}^{-1} \end{bmatrix} \succ \mathbf{0}. \end{aligned} \quad (24)$$

With the following change of variables

$$\bar{\mathbf{P}} := \mathbf{P}^{-1}, \quad \bar{\mathbf{A}}_c := \mathbf{P}^{-1}\hat{\mathbf{A}}_c, \quad \bar{\mathbf{L}}_c := \mathbf{P}^{-1}\hat{\mathbf{L}}_c, \quad (25)$$

we can formulate a set of LMIs given by

$$\begin{aligned} & \min_{\bar{\mathbf{P}}, \bar{\mathbf{A}}_c, \bar{\mathbf{L}}_c} \|\bar{\mathbf{P}}\mathbf{X}_1 - \bar{\mathbf{A}}_c\|_F^2 \\ & \text{subject to: } \begin{bmatrix} \bar{\mathbf{P}} & \bar{\mathbf{A}}_c + \bar{\mathbf{L}}_c \hat{\mathbf{C}}_s \\ \star & \bar{\mathbf{P}} \end{bmatrix} \succ 0. \end{aligned} \quad (26)$$

Essentially, this proves the following theorem.

Theorem 1. *Suppose Assumptions 1–2 hold. If there exists matrices $\bar{\mathbf{A}}_c$, $\bar{\mathbf{L}}_c$, and $\bar{\mathbf{P}} = \bar{\mathbf{P}}^\top \succ 0$ such that (26) holds, then the observer*

$$\mathbf{z}_{k+1}^c = \hat{\mathbf{A}}_c \mathbf{z}_k^c + \hat{\mathbf{B}}_c u_k + \hat{\mathbf{L}}_c (\hat{\mathbf{C}}_s \mathbf{z}_k^c - \mathbf{y}_k) \quad (27)$$

with state matrix $\hat{\mathbf{A}}_c = \bar{\mathbf{P}}^{-1} \bar{\mathbf{A}}_c$, $\hat{\mathbf{B}}_c = \mathbf{X}_2$ and observer gain $\hat{\mathbf{L}}_c = \bar{\mathbf{P}}^{-1} \bar{\mathbf{L}}_c$ exhibits error dynamics that are asymptotically stable, that is, $\mathbf{z}_k^c \rightarrow \hat{\mathbf{x}}_k$ as $k \rightarrow \infty$.

The pseudocode for exact co-design is provided in Algorithm 2.

Algorithm 2 Exact Co-design

Require: Data, \mathbf{X}_+ , $\bar{\mathbf{X}}$

Require: Output matrix, \mathbf{C}

Require: Target state dimension, r_x

Require: Truncated SVD subroutine, $[\mathbf{U}, \mathbf{\Sigma}, \mathbf{V}] = \text{svd}(\cdot, \cdot)$

$[\hat{\mathbf{U}}, \sim, \sim] = \text{svd}(\mathbf{X}_+, r_x)$

Partition data using (22)

Compute $\hat{\mathbf{C}}_s$ using (14)

Solve the SDP (26) for $\bar{\mathbf{P}}$, $\bar{\mathbf{A}}_c$, and $\bar{\mathbf{L}}_c$

Compute $\hat{\mathbf{A}}_c = \bar{\mathbf{P}}^{-1} \bar{\mathbf{A}}_c$

Compute $\hat{\mathbf{L}}_c = \bar{\mathbf{P}}^{-1} \bar{\mathbf{L}}_c$

return $\hat{\mathbf{A}}_c$, $\hat{\mathbf{B}}_c = \mathbf{X}_2$, $\hat{\mathbf{L}}_c$

4.2. Burer-Monteiro Heuristics for Large-Scale LMIs

To obtain a good fit, the required model order may be large, that is, r_x is large. Therefore, the set of LMI conditions (26) may be large, implying that state-of-the-art SDP solvers based on interior point methods may require prohibitive time to solve the co-design problem exactly. In fact, the worst-case computational complexity incurred by solving an SDP with $m \times m$ matrices has been reported to be $\mathcal{O}(m^{6.5})$ [36]. For such cases, we propose the use of Burer-Monteiro methods [37] to provide a tractable algorithm for computing an approximate solution to (26). Note that these approximations typically result in suboptimal solutions, but are scalable to high-dimensional SDPs. Heuristics based on Burer-Monteiro methods are discussed next. Let

$$\mathbf{F} = \begin{bmatrix} \bar{\mathbf{P}} & \bar{\mathbf{A}}_c + \bar{\mathbf{L}}_c \hat{\mathbf{C}}_s \\ \star & \bar{\mathbf{P}} \end{bmatrix}$$

denote the left hand side of the matrix inequality in (26). Suppose that there exists a matrix $\mathbf{\Xi}$ such that $\mathbf{F} = \mathbf{\Xi}\mathbf{\Xi}^\top$. Therefore, $\text{rank}(\mathbf{F}) = \text{rank}(\mathbf{\Xi})$. Since any feasible solution to the co-design LMI requires $\mathbf{F} \succ 0$, \mathbf{F} needs to be full rank.

Let \mathbf{F} have the block representation

$$\mathbf{F} = \begin{bmatrix} \mathbf{F}_1 & \mathbf{F}_2 \\ \mathbf{F}_2^\top & \mathbf{F}_3 \end{bmatrix}.$$

Therefore, comparing blocks, we have $\mathbf{F}_1 = \bar{\mathbf{P}}$, $\mathbf{F}_2 = \bar{\mathbf{A}}_c + \bar{\mathbf{L}}_c \hat{\mathbf{C}}_s$, and $\mathbf{F}_3 = \bar{\mathbf{P}}$. Following the philosophy of Burer-Monteiro methods, we define Ξ as the decision variable matrix. Using Ξ we can replace the co-design objective by constructing \mathbf{F} using the outer product $\Xi \Xi^\top$, and recasting the problem (26) as

$$\min_{\Xi, \bar{\mathbf{L}}_c} \|\mathbf{F}_1 \mathbf{X}_1 - \mathbf{F}_2 + \bar{\mathbf{L}}_c \hat{\mathbf{C}}_s\|_{\mathbb{F}}^2 + \|\mathbf{F}_3 - \mathbf{F}_1\|_{\mathbb{F}}^2 =: J \quad (28)$$

since $\bar{\mathbf{P}} = \mathbf{F}_1$, and $\bar{\mathbf{A}}_c = \mathbf{F}_2 + \bar{\mathbf{L}}_c \hat{\mathbf{C}}_s$. The distance between \mathbf{F}_1 and \mathbf{F}_3 needs to be minimized in order to ensure they are both identical to $\bar{\mathbf{P}}$.

The approximated co-design problem (28) can be solved using gradient-based methods. In particular, the gradients of $f(\mathbf{U}, \bar{\mathbf{L}}_c)$ with respect to \mathbf{U} and $\bar{\mathbf{L}}_c$ are given by

$$\begin{aligned} \nabla_{\Xi} J &= \begin{bmatrix} \nabla_{\Xi} J_{11} & \nabla_{\Xi} J_{12} \\ \star & \nabla_{\Xi} J_{22} \end{bmatrix}, \\ \nabla_{\bar{\mathbf{L}}_c} J &= (\mathbf{F}_1 \mathbf{X}_1 - \mathbf{F}_2 + \bar{\mathbf{L}}_c \hat{\mathbf{C}}_s \mathbf{F}_1)(\hat{\mathbf{C}}_s \mathbf{F}_1)^\top, \end{aligned}$$

where

$$\begin{aligned} \nabla_{\Xi} J_{11} &= (\mathbf{F}_1 \mathbf{X}_1 - \mathbf{F}_2 + \bar{\mathbf{L}}_c \hat{\mathbf{C}}_s \mathbf{F}_1)(\mathbf{X}_1 + \bar{\mathbf{L}}_c \hat{\mathbf{C}}_s)^\top - 2(\mathbf{F}_3 - \mathbf{F}_1), \\ \nabla_{\Xi} J_{12} &= -\mathbf{X}_1 \mathbf{F}_3 + \mathbf{F}_2 - \bar{\mathbf{L}}_c \hat{\mathbf{C}}_s \mathbf{F}_3, \\ \nabla_{\Xi} J_{22} &= \mathbf{F}_3 \mathbf{X}_1 - \mathbf{F}_2 + \bar{\mathbf{L}}_c \hat{\mathbf{C}}_s \mathbf{F}_3)(\mathbf{X}_1 + \bar{\mathbf{L}}_c \hat{\mathbf{C}}_s)^\top + 2(\mathbf{F}_3 - \mathbf{F}_1). \end{aligned}$$

Since this problem has a large number of decision variables (all the elements of Ξ), we use a scalable, low-memory quasi-Newton method called L-BFGS for solving this problem; c.f. [38]. The pseudocode is provided in Algorithm 3.

Algorithm 3 Co-design with Burer-Monteiro Heuristics

Require: Data, \mathbf{X}_+ , $\bar{\mathbf{X}}$
Require: Output matrix, \mathbf{C}
Require: Target state dimension, r_x
Require: Truncated SVD subroutine, $[\mathbf{U}, \Sigma, \mathbf{V}] = \text{svd}(\cdot, \cdot)$
Require: Full rank Ξ
 $[\hat{\mathbf{U}}, \sim, \sim] = \text{svd}(\mathbf{X}_+, r_x)$
 Compute $\hat{\mathbf{C}}_s$ using (14)
 Solve (28) using L-BFGS with $\mathbf{F} = \Xi \Xi^\top$
 Partition \mathbf{F} into $\mathbf{F}_1, \mathbf{F}_2, \mathbf{F}_3$
 Compute $\mathbf{P} = \mathbf{F}_1^{-1}$
 Compute $\bar{\mathbf{L}}_c = \bar{\mathbf{P}}^{-1} \bar{\mathbf{L}}_c$
 Compute $\mathbf{A}_c = \mathbf{F}_2 - \bar{\mathbf{L}}_c \hat{\mathbf{C}}_s$
return $\mathbf{A}_c, \mathbf{B}_c, \bar{\mathbf{L}}_c$

5. Results and Discussion

In this section, we compare the proposed co-design algorithm with a sequential design approach. We begin by describing the numerical solver and the data collection methodology. Subsequently, we demonstrate that even for the simpler Advection Diffusion equation, the sequential design pipeline may result in instability of the observer. Finally, we show that the co-design eliminates this problem, and we illustrate the effectiveness of the co-designed system on the more challenging Boussinesq equations. All simulations are executed on an Intel Core *i5* CPU with 8 GB RAM.

5.1. Data Collection

5.1.1. Advection Diffusion PDEs

We used the method of lines to approximately solve the advection-diffusion system; see Section 2.1.1 for the complete description and notation. Obtaining solutions for the Advection Diffusion PDEs involves discretizing the spatial domain Ω and replacing the PDE with a system of ordinary differential equations (ODEs), which can then be integrated in time. For the spatial discretization, we developed a stencil matrix A based on finite volume methods. For the convection terms, we use second-order Gaussian integration, and for diffusion equations we use Gaussian integration with central-difference-interpolation. The computational domain Ω is represented by a 50×50 grid such that $T(\mathbf{x}, t)$ is a 2500 dimensional real-valued vector. For the purpose of mesh sensitivity analysis, we used a finer grid of 100×100 , which resulted in essentially the same behaviour. Finally, we used MATLAB's `ode45` for generating the snapshots. We generate 2000 snapshots, sampled at every 0.5 s, for 1000 s. The initial temperature for simulation was set to be 230K uniformly. No exogenous input was added to the system, but boundary condition noise produced excitory dynamics.

5.1.2. Boussinesq PDEs

For numerical solution of the Boussinesq system (4), we use `OpenFOAM` [39], an open-source object-oriented finite-volume based CFD software with a collocated grid arrangement. The solver is based on the `OpenFOAM` native solver `buoyantBoussinesqPimpleFoam`. Pressure and velocity are decoupled using the `SIMPLE` algorithm [40]. For the convection terms, we use second order Gaussian integration with the Sweby limiter to account for propagation of density fronts, and numerical stability. For diffusion, we use Gaussian integration with central-differencing-interpolation. The advective terms in the energy equation are discretized using the second order upwind scheme of the van Leer method. The time integration was performed with the implicit Crank-Nicolson method, which is second-order bounded. The discretized algebraic equations are solved using the Preconditioned biconjugate gradient method. The mesh sensitivity analysis is performed to ensure independence of results from the number of nodes. The dataset is generated with initial conditions at 251 K for temperature (uniformly) and airflow velocity is zero. This replicates a common real-world condition for quiescent rooms. The sampling time for collecting the snapshots is chosen to be 0.5 s, in accordance with the Nyquist-Shannon sampling theorem. Furthermore, we verify via numerical simulations that such a sampling time is much smaller than the initial transients for both temperature and velocity fields to ensure that the collected snapshots capture the relevant dynamics. We selected one temperature sensor for this simulation, whose location is at the boundary of the left and right large circulations (see Fig. 1) adjacent to the bottom wall, as representative of coherent structures consistent with [41]. We set the time horizon of simulations to be long enough time to capture all the dominant phenomena. The CFD simulations illustrate that the time horizon is well beyond the settling times of the relevant dynamics. Our solver has been verified for various buoyancy-driven application within the built environment and more details can be found in [31, 42]. The same integration time step was used as in the previous example, and the inputs were boundary condition noise, snapshots are collected as the system's transients decay and the system reaches steady-state.

5.2. Instability with Sequential Design: Illustrative Example

Even for the linear Advection Diffusion system, we see that the sequential method does not always succeed. Based on the data obtained from this system we employ Algorithm 1 for a sequential design and Algorithm 2 for an exact co-design. Figure 2 shows a subset of the eigenvalues of $(\mathbf{A}_s + \mathbf{L}_s \mathbf{C}_s)$ (corresponding to the highest magnitude) for i) sequential design and exact co-design. It is apparent that, for the sequential case, a pair of eigenvalues (blue) lie outside the unit circle (cyan, dashed) rendering the discrete-time estimation error dynamics of the observer (15) unstable. Conversely, the co-design eigenvalues (red) based observer (27) results in stable error dynamics.

5.3. Numerical Results for Boussinesq System

In this section, we consider the problem of jointly estimating the model and observer for the Boussinesq system described in Section 2.1.2.

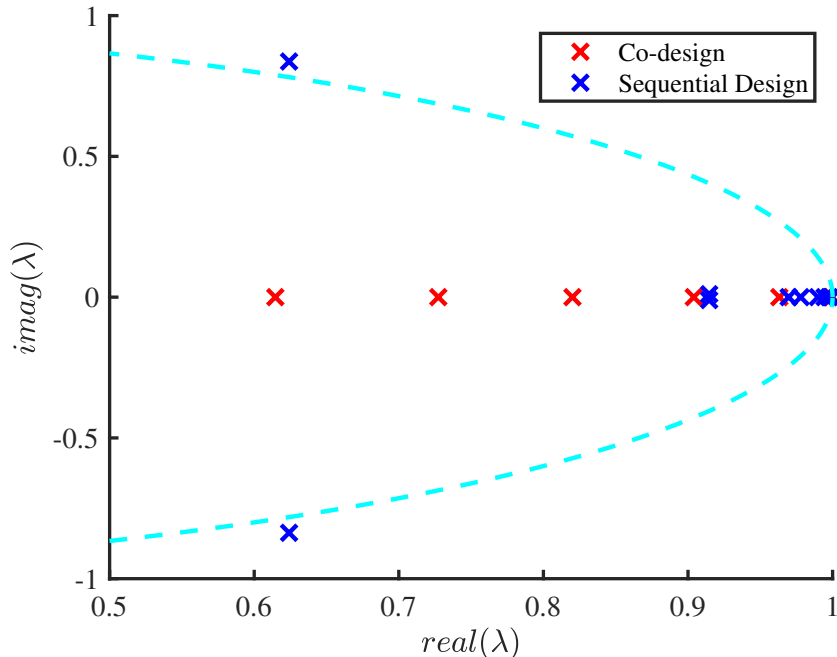


Figure 2: Eigenvalue map of $(\mathbf{A}_s + \mathbf{L}_s \mathbf{C}_s)$ for sequential design and exact co-design. Only the highest magnitude poles are shown. A slice of the unit circle is shown with dashed cyan lines.

Sequential Design. We apply DMDc (Algorithm 1) to our dataset. The dimension of the data-set is 39,600 with the full-order model. The target dimension found for the algorithm is $r_x = 34$, which is a reduction of three orders of magnitude. The resulting system matrices are then used to compute a Luenberger observer following Algorithm 1. If DMDc results in no instabilities, this procedure is quite straight-forward and inexpensive, but empirically, we found that this method fails quite often as the observer generated does not exhibit desired stability properties.

Co-design. We follow the procedure presented in Section 4 for jointly computing the system matrices and observer. Specifically, we use Algorithm 3 to solve the co-design SDP via `scipy.optimize`. L-BFGS maintains a history of the past m updates of the decision variables and gradient; we use $m = 10$. The gradient is computed using `autograd` which is intrinsic to `scipy.optimize`.

L-BFGS can handle much larger problems than classical quasi-newton methods due to its inherently low memory usage. However, it is still difficult to solve the problem in hand (start dimension = 39600). The state dimension is thus reduced to 100 using a truncated SVD. It is worth noting that although the state-space is relatively small ($r_x = 100$), the variable space for the optimization problem (26) is 20100, which is too large for standard solvers like `CVX` or `YALMIP`. The progress of the L-BFGS algorithm is measured using a Euclidean norm of the gradient. When this Euclidean norm is below $\epsilon = 10^{-3}$, we terminate the algorithm.

Figure 3 shows results pertaining to model identification. The top plot shows the temperature profile at 100 unique locations in the room. The bottom plot shows the relative error¹ for the sequential and co-design models against CFD simulations: it is clear that our proposed co-design method has significantly lower relative error compared to sequential design. Both of these results indicate that the model obtained using co-design is in good agreement with the generated data. From the bottom subplot, we see that the co-design model has very small relative error with respect to the CFD data. This is a beneficial property of the

¹Relative error % = $100 \times (\text{CFD data} - \text{ROM outputs}) / \text{CFD data}$

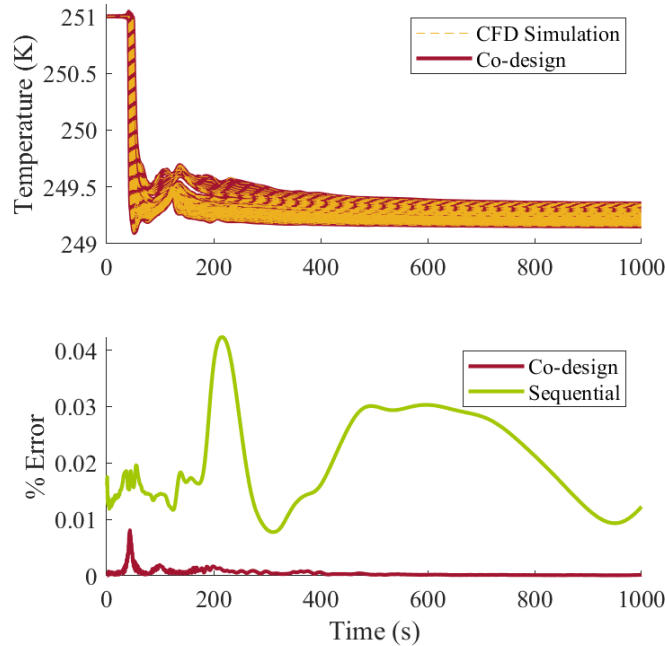


Figure 3: (Top) Temperature profiles of 100 different locations in the room. (Bottom) Relative error % for both methods with respect to the given CFD simulation data.

co-design; note however, that this does not imply that the model identified is exactly the same as the CFD model, since this low relative error is for a specific location in the room. The extrapolative properties of the model will be illustrated via the state estimation plots later in this subsection. This is further corroborated with the contour plot shown in Figure 4. Here, we consider snapshots of the simulation at various times. The flow is originated from the top boundary, and due to the momentum and the gravitational forces, the cold air starts to mix with the ambient. In the process, large vortical patterns form at the tip of inlet, which intensify the mixing. After some time, say $t = 200$, there is clear subdivision between left and right of the room, which now exhibit temperature disparities. We see that the distribution of temperature at each time is closely captured in the top plot (co-design) in relation to the bottom (CFD simulation). More importantly, vital features of flow, such as the boundary of left/colder to the right/warmer region is fully captured in the results of ROMs obtained by co-design.

Figure 5 shows the relative estimation error % for the sequential and co-design models against CFD simulations. The co-design method has significantly lower relative estimation error as compared to sequential. While both sequential and co-design demonstrate non-zero final estimation error after 600 s, that is because the identified model has a mismatch with the true dynamics. While the code-design finishes with an estimate that exhibits small drift, the sequential estimate worsens with time and starts to demonstrate instability, further motivating the use of co-design methods in practice. A time-wise comparison of state estimation with only the co-design observer is illustrated in Fig. 6. From $t = 10$ s, note that the initial conditions of the observer and the system are not identical. While there are certainly state estimation errors in specific temperature values, it is clear the overall trends are quite similar over the transient. At quasi-steady-state ($t = 1500$ s), the performance of the observer is excellent and visual inspection of the bottom right subplot yields no discernible differences even at the corners of the space, demonstrating the potential of the co-design method.

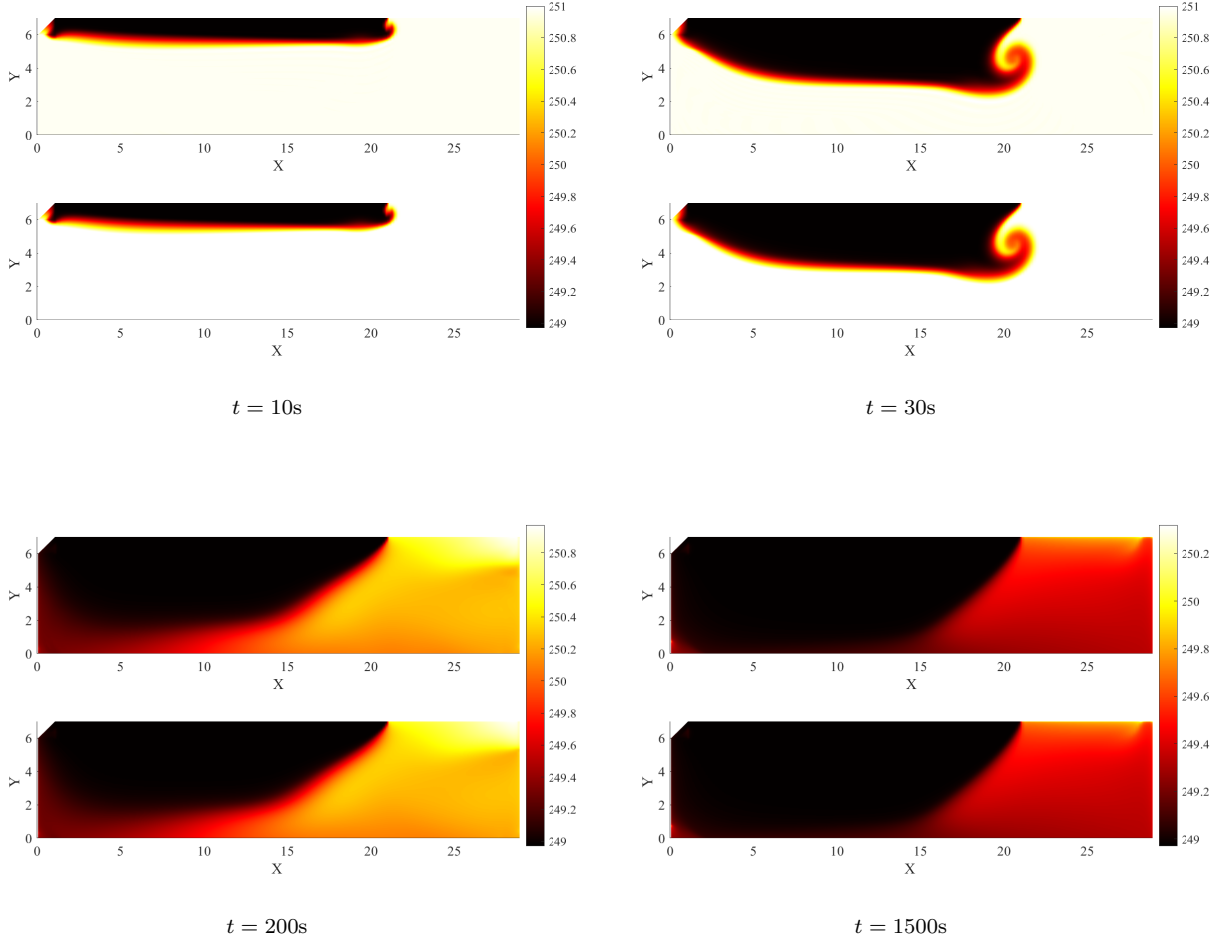


Figure 4: *Model Fit*: Temperature distribution in the room at various times in the simulation. In each subplot, we show simulations for identified model using co-design (upper) and the true model (lower).

6. Conclusions

The problem of estimating fully turbulent flows, described by Boussinesq equations is studied in presence of uncertainties such as disturbance inputs on walls and unmodeled dynamics. Due to the large-scale system at hand, which are in turn result of discretized PDEs, a dynamic mode decomposition method is used for identifying a reduced-order state-space model that enables estimator design. An advantage of our proposed approach is that the model is constructed directly from data, and does not require the direct solution of Boussinesq equations which would make the problem intractable on-line due to scalability issues. Based on the DMDc model, we propose sequential and simultaneous co-design formulations for model identification and observer design. We demonstrate that even with simpler PDEs like the Advection Diffusion system, sequential design may result in instabilities of the state estimation error dynamics, which is eliminated with co-design. Since the co-design results in a complex optimization problem that is not tractable with standard SDP solvers, we propose heuristics for enabling the solution of such problems based on quasi-Newton approaches. Our proposed methodology can also be used in a wide range of applications involving large-scale systems that exhibit turbulent flows such as drag reduction in aerospace systems and wind energy systems.

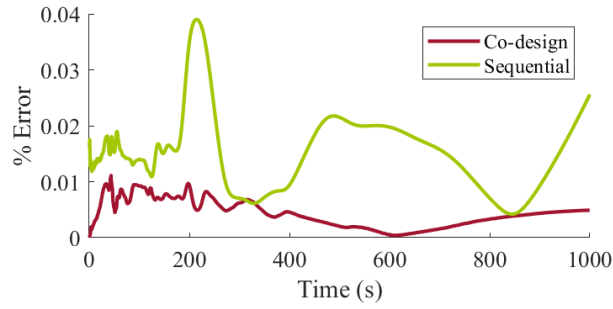


Figure 5: *Estimation*: Relative estimation error % for both sequential and co-design methods.

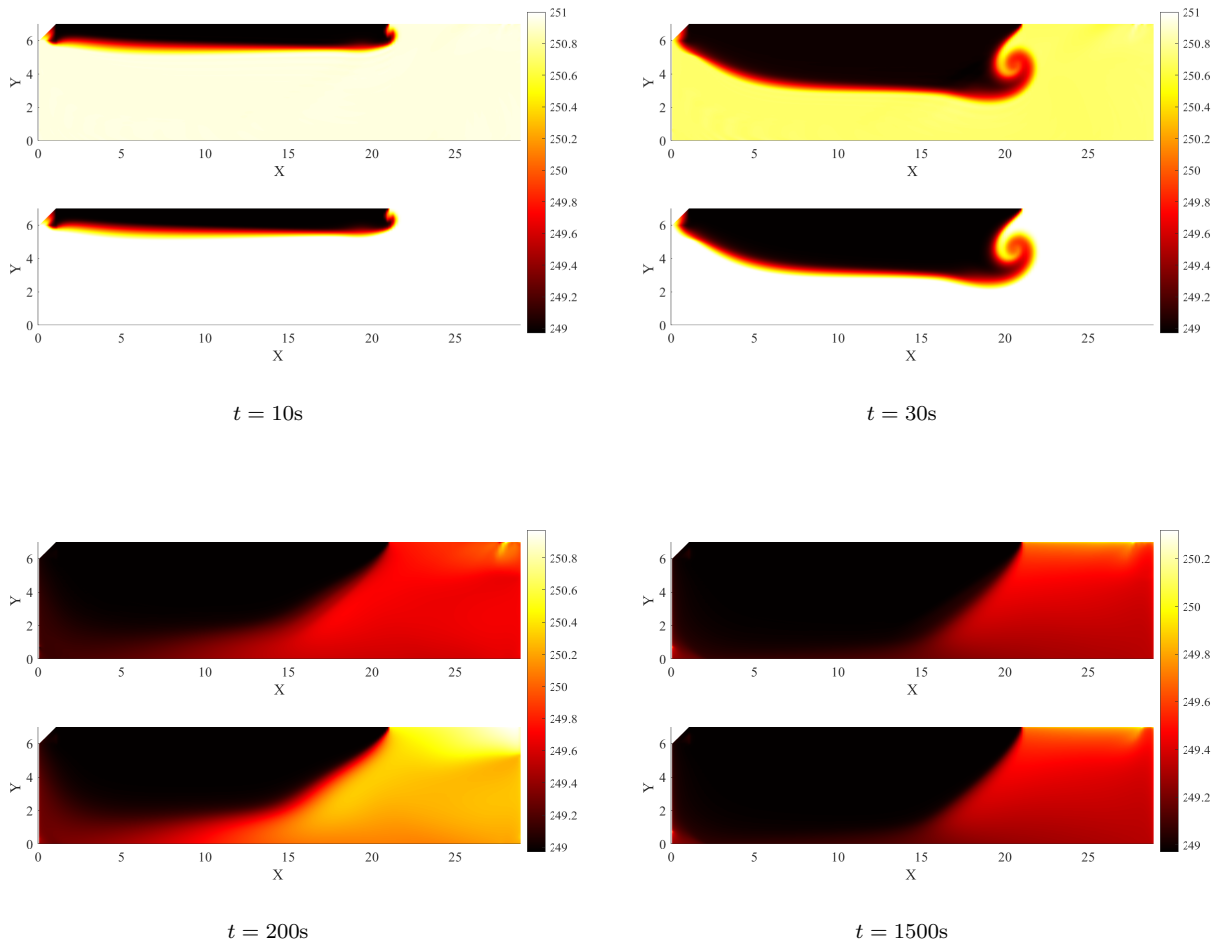


Figure 6: *Estimation*: Temperature distribution in the room at various times in the simulation. In each case, we show the estimated state using co-design (top) and the true temperature (bottom).

References

- [1] O. Brastein, D. Perera, C. Pfeifer, and N.-O. Skeie, "Parameter estimation for grey-box models of building thermal behaviour," *Energy Build.*, vol. 169, pp. 58–68, jun 2018. [Online]. Available: <https://doi.org/10.1016/j.enbuild.2018.03.057><https://linkinghub.elsevier.com/retrieve/pii/S0378778817331791>

- [2] J. Borggaard, J. A. Burns, A. Surana, and L. Zietsman, "Control, estimation and optimization of energy efficient buildings," in *Proc. of the American Control Conference (ACC)*, 2009, pp. 837–841.
- [3] C. R. Laughman, C. Mackey, S. A. Bortoff, and H. Qiao, "Modeling and Control of Radiant, Convective, and Ventilation Systems for Multizone Residences," *Building Simulation Conference*, pp. 1956–1963, 2019.
- [4] Y. Zhou, M. Wang, M. Wang, and Y. Wang, "Predictive accuracy of Boussinesq approximation in opposed mixed convection with a high-temperature heat source inside a building," *Building and Environment*, vol. 144, pp. 349–356, 2018.
- [5] N. Ivanov and M. Zsimeva, "Large eddy simulation of airflow in a test ventilated room," in *Journal of Physics: Conference Series*, vol. 1038, no. 1. IOP Publishing, 2018, p. 012136.
- [6] J. R. Singler, "New POD error expressions, error bounds, and asymptotic results for reduced order models of parabolic PDEs," *SIAM Journal on Numerical Analysis*, vol. 52, no. 2, pp. 852–876, 2014.
- [7] P. J. Schmid, "Dynamic mode decomposition of numerical and experimental data," *Journal of fluid mechanics*, vol. 656, pp. 5–28, 2010.
- [8] J. N. Kutz, S. L. Brunton, B. W. Brunton, and J. L. Proctor, *Dynamic mode decomposition: data-driven modeling of complex systems*. SIAM, 2016.
- [9] S. E. Otto and C. W. Rowley, "Koopman operators for estimation and control of dynamical systems," *Annual Review of Control, Robotics, and Autonomous Systems*, vol. 4, 2021.
- [10] H. Arbabi and I. Mezic, "Ergodic theory, dynamic mode decomposition, and computation of spectral properties of the Koopman operator," *SIAM Journal on Applied Dynamical Systems*, vol. 16, no. 4, pp. 2096–2126, 2017.
- [11] M. Guay and N. Hariharan, "Airflow velocity estimation in building systems," in *American Control Conference*, 2009, pp. 908–913.
- [12] T. John, M. Guay, N. Hariharan, and S. Narayanan, "POD-based observer for estimation in Navier–Stokes flow," *Computers & Chemical Engineering*, vol. 34, no. 6, pp. 965–975, 2010.
- [13] W. MacKunis, S. Drakunov, M. Reyhanoglu, and L. Ukeiley, "Nonlinear estimation of fluid velocity fields," in *Proc. of the IEEE Conf. on Decision and Control*, 2011, pp. 6931–6935.
- [14] S. Koga, M. Benosman, and J. Borggaard, "Learning-based robust observer design for coupled thermal and fluid systems," in *American Control Conference (ACC)*, July 2019, pp. 941–946.
- [15] A. Chakrabarty and M. Benosman, "Safe learning-based observers for unknown nonlinear systems using Bayesian optimization," *Automatica*, vol. 133, p. 109860, 2021.
- [16] M. Benosman and J. Borggaard, "Robust nonlinear state estimation for thermal-fluid models using reduced-order models: The case of the Boussinesq equations," in *Proc. of the IEEE Conf. on Decision and Control*, December 2019.
- [17] A. Chakrabarty, A. Zemouche, R. Rajamani, and M. Benosman, "Robust data-driven neuro-adaptive observers with Lipschitz activation functions," in *2019 IEEE 58th Conference on Decision and Control (CDC)*, 2019, pp. 2862–2867.
- [18] S. Vijayshankar, S. Nabi, A. Chakrabarty, P. Grover, and M. Benosman, "Dynamic mode decomposition and robust estimation: Case study of a 2D turbulent Boussinesq flow," in *Proc. of the 2020 American Control Conference (ACC)*, 2020, pp. 2351–2356.
- [19] H. Fathy, P. Papalambros, and A. Ulsoy, "On combined plant and control optimization," in *8th Cairo University International Conference on Mechanical Design and Production, Cairo University*, 2004.
- [20] J. T. Allison, T. Guo, and Z. Han, "Co-design of an active suspension using simultaneous dynamic optimization," *Journal of Mechanical Design*, vol. 136, no. 8, 2014.
- [21] R. Patil, Z. Filipi, and H. Fathy, "Computationally efficient combined design and control optimization using a coupling measure," *IFAC Proceedings Volumes*, vol. 43, no. 18, pp. 144–151, 2010.
- [22] M.-J. Kim and H. Peng, "Power management and design optimization of fuel cell/battery hybrid vehicles," *Journal of power sources*, vol. 165, no. 2, pp. 819–832, 2007.
- [23] H. K. Fathy, P. Y. Papalambros, A. G. Ulsoy, and D. Hrovat, "Nested plant/controller optimization with application to combined passive/active automotive suspensions," in *Proceedings of the 2003 American Control Conference, 2003.*, vol. 4. IEEE, 2003, pp. 3375–3380.
- [24] W. Jeon, A. Chakrabarty, A. Zemouche, and R. Rajamani, "Simultaneous state estimation and tire model learning for autonomous vehicle applications," *IEEE/ASME Transactions on Mechatronics*, vol. 26, no. 4, pp. 1941–1950, 2021.
- [25] N. A. Diangelakis, B. Burnak, J. Katz, and E. N. Pistikopoulos, "Process design and control optimization: A simultaneous approach by multi-parametric programming," *AIChE Journal*, vol. 63, no. 11, pp. 4827–4846, 2017.
- [26] M. J. Abzug and E. E. Larrabee, *Airplane stability and control: a history of the technologies that made aviation possible*. Cambridge University Press, 2005, vol. 14.
- [27] V. Sakizlis, J. D. Perkins, and E. N. Pistikopoulos, "Parametric controllers in simultaneous process and control design optimization," *Industrial & Engineering Chemistry Research*, vol. 42, no. 20, pp. 4545–4563, 2003.
- [28] A. L. Nash and N. Jain, "Combined plant and control co-design for robust disturbance rejection in thermal-fluid systems," *IEEE Transactions on Control Systems Technology*, vol. 28, no. 6, pp. 2532–2539, 2019.
- [29] —, "Hierarchical control co-design using a model fidelity-based decomposition framework," *Journal of Mechanical Design*, vol. 143, no. 1, 2021.
- [30] S. Burer and R. D. Monteiro, "A nonlinear programming algorithm for solving semidefinite programs via low-rank factorization," *Mathematical Programming*, vol. 95, no. 2, pp. 329–357, 2003.
- [31] S. Nabi, P. Grover, and P. C.-C. Caulfield, "Adjoint-based optimization of displacement ventilation flow," *Building and Environment*, vol. 124, pp. 342–356, 2017.
- [32] S. L. Lacy and D. S. Bernstein, "Subspace identification with guaranteed stability using constrained optimization," *IEEE Transactions on Automatic Control*, vol. 48, no. 7, pp. 1259–1263, 2003.
- [33] L. Ljung, "System identification," *Wiley Encyclopedia of Electrical and Electronics Engineering*, pp. 1–19, 1999.

- [34] J. L. Proctor, S. L. Brunton, and J. N. Kutz, “Dynamic mode decomposition with control,” *SIAM J. Applied Dynamical Systems*, vol. 15, no. 1, pp. 142–161, 2016.
- [35] S. Boyd, L. El Ghaoui, E. Feron, and V. Balakrishnan, *Linear Matrix Inequalities In System And Control Theory*. SIAM, 1994.
- [36] Y. Nesterov, *Introductory lectures on convex optimization: A basic course*. Springer Science & Business Media, 2013, vol. 87.
- [37] N. Boumal, V. Voroninski, and A. Bandeira, “The non-convex burer-monteiro approach works on smooth semidefinite programs,” *Advances in Neural Information Processing Systems*, vol. 29, pp. 2757–2765, 2016.
- [38] D. C. Liu and J. Nocedal, “On the limited memory bfgs method for large scale optimization,” *Mathematical programming*, vol. 45, no. 1, pp. 503–528, 1989.
- [39] H. Jasak, “Openfoam: open source CFD in research and industry,” *International Journal of Naval Architecture and Ocean Engineering*, vol. 1, no. 2, pp. 89–94, 2009.
- [40] S. Patankar, *Numerical heat transfer and fluid flow*. Taylor & Francis, 2018.
- [41] A. Surana, N. Hariharan, S. Narayanan, and A. Banaszuk, “Reduced order modeling for contaminant transport and mixing in building systems: A case study using dynamical systems techniques,” in *2008 American Control Conference*. IEEE, 2008, pp. 902–907.
- [42] S. Nabi, P. Grover, and C. Caulfield, “Nonlinear optimal control strategies for buoyancy-driven flows in the built environment,” *Computers & Fluids*, vol. 194, p. 104313, 2019.